

Article

Side-Chain Labeling Strategy for Forming Self-Sorted Columnar Liquid Crystals from Binary Discotic Systems

Tsuneaki Sakurai ^{1,*} , Kenichi Kato ² and Masaki Shimizu ¹

¹ Faculty of Molecular Chemistry and Engineering, Kyoto Institute of Technology, Hashikami-cho, Matsugasaki, Sakyo-ku, Kyoto 606-8585, Japan

² RIKEN SPring-8 Center, 1-1-1 Kouto, Sayo-cho, Sayo-gun 679-5148, Japan

* Correspondence: sakurai@kit.ac.jp

Abstract: The spontaneous formation of self-sorted columnar structures of electron-donating and accepting π -conjugated molecules is attractive for photoconducting and photovoltaic properties. However, the simple mixing of donor–acceptor discotic molecules usually results in the formation of mixed-stacked or alternating-stacked columns. As a new strategy for overcoming this problem, here, we report the “side-chain labeling” approach using binary discotic systems and realize the preferential formation of such self-sorted columnar structures in a thermodynamically stable phase. The demonstrated key strategy involves the use of hydrophobic and hydrophilic side chains. The prepared blend is composed of liquid crystalline phthalocyanine with branched alkyl chains (H_2Pc) and perylene diimide (PDI) carrying alkyl chains at one side and triethyleneglycol (TEG) chains at the other side ($PDI_{C12/TEG}$). To avoid the thermodynamically unfavorable contact among hydrophobic and hydrophilic chains, $PDI_{C12/TEG}$ self-assembles to stack up on top of each other and H_2Pc as well, forming a homo-stacked pair of columns (self-sort). Importantly, H_2Pc and $PDI_{C12/TEG}$ in the blend are macroscopically miscible and uniform, and mesoscopically segregated. The columnar liquid crystalline microdomains of H_2Pc and $PDI_{C12/TEG}$ are homeotropically aligned in a glass sandwiched cell. The “labeling” strategy demonstrated here is potentially applicable to any binary discotic system and enables the preferential formation of self-sorted columnar structures.

Keywords: self-sort; segregated columns; binary mixture; amphiphilicity; homeotropic alignment



Citation: Sakurai, T.; Kato, K.; Shimizu, M. Side-Chain Labeling Strategy for Forming Self-Sorted Columnar Liquid Crystals from Binary Discotic Systems. *Crystals* **2023**, *13*, 1473. <https://doi.org/10.3390/cryst13101473>

Academic Editor: Benoit Heinrich

Received: 27 August 2023

Revised: 6 October 2023

Accepted: 7 October 2023

Published: 10 October 2023



Copyright: © 2023 by the authors. Licensee MDPI, Basel, Switzerland. This article is an open access article distributed under the terms and conditions of the Creative Commons Attribution (CC BY) license (<https://creativecommons.org/licenses/by/4.0/>).

1. Introduction

The control of nanostructures and miscibility of binary blends is important for tuning the physical properties of the blended organic materials. Historically, polymer blend has been a famous notion, where the miscibility and compatibility of blended polymers have been well discussed, especially in view of their effect on thermal and mechanical properties [1–4]. The bulk heterojunction of conjugated polymers and fullerene derivatives is another famous concept utilized for blend films in organic photovoltaic cells [5–7]. More recently, blends of electron donors and acceptors based on conjugated polymers or small molecules have been used for active layers in organic electronic devices, including photovoltaic cells [8–10], electrochemical transistors [11], ambipolar transistors [12], and so on. In these blends, not only large interfaces of donor and acceptor molecules (or macromolecules) but also hole/electron-transporting bicontinuous interpenetrating networks are essential for the device operation. The optimization of such nanostructures in the blends is usually performed by a try-and-error approach using spin-coating methods. Meanwhile, hydrogen-bond-assisted organogelator systems have been demonstrated as a more elaborated molecular design [13–16]. In these systems, self-sorted fibrous one-dimensional assemblies were developed by the simple mixing of electron donor and acceptor molecules. The different distances of two hydrogen bonding sites between the donor and acceptor molecules are critical for the formation of self-sorting fibers. Although methodologies of

bulk heterojunctions as well as binary organogelator systems have been established, they have a critical drawback: the obtained nanostructures are kinetically controlled but not thermodynamically stable in the long term. Thus, the construction of thermodynamic bicontinuous structures of electron donor and acceptor materials has been awaited.

Liquid crystal (LC) phases are usually thermodynamically stable and appropriate as a platform for constructing the arrays of π -conjugated systems through self-assembly, resulting in the functional soft materials [17–23]. However, there has been no example of binary LC blends with bicontinuous structures. In columnar LC phases of discotic π -systems, columnarly stacked π -conjugated molecules enable one-dimensional charge transport pathways. If electron-donating and accepting π -conjugated molecules form a self-sorted columnar structure, we can realize intracolumnar hole/electron transport pathways as well as intercolumnar p/n heterojunctions with large interfaces, which equips a long-term structural stability. However, in relevant previous studies, mixed-stacking columnar structures were reported from LC phthalocyanine (p -type: electron donor) and perylene diimide (PDI) (n -type: electron acceptor) molecules [24–26]. This is quite reasonable because they are entropically favored (Figure 1a). Special molecular designs are required to accomplish thermodynamically stable self-sorted columnar structures by the self-assembly of LC electron donor and acceptor molecules. Here, we report a “side-chain labeling” strategy to realize self-sorted columnar structures from LC mixtures composed of free-base phthalocyanine (H_2Pc) and PDI derivatives $PDI_{C12/C12}$, $PDI_{C12/TEG}$, and $PDI_{TEG/TEG}$ (Figure 2). The dissymmetric introduction of both hydrophobic and hydrophilic side chains in $PDI_{C12/TEG}$ gives large enthalpic gain to the homo-stacked PDI columns, and thus the self-sorted structure is stabilized when the $PDI_{C12/TEG}$ is mixed with H_2Pc carrying hydrophobic chains (Figure 1b). Furthermore, the resulting self-sorted LC columns of the $PDI_{C12/TEG}$ and H_2Pc molecules align homeotropically in a sandwiched glass cell, which is desirable for efficient charge transport in photovoltaic applications.

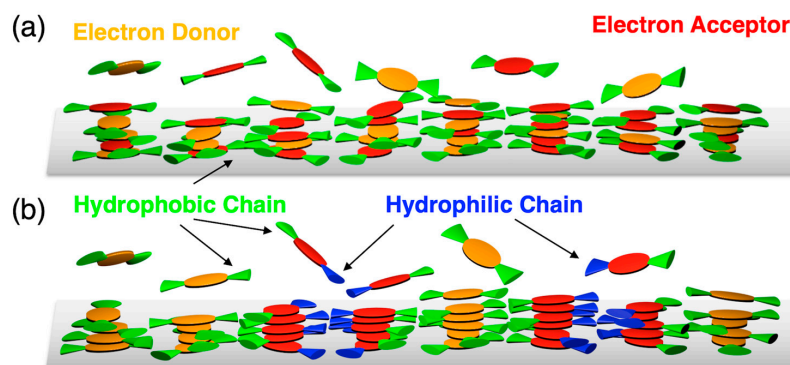


Figure 1. Schematic illustrations of side-chain-directed molecular assembly of electron donors (orange) and acceptor (red) π -systems (a) substituted with hydrophobic side chains (green) alone and (b) site-specifically substituted with hydrophobic (green) and hydrophilic (blue) side chains.

Entropically favored mixed-stacking structures can be formed because both electron donor and acceptor molecules are decorated with alkyl chains and they are molecularly miscible. We focused on strong enthalpic interactions of immiscible hydrophobic and hydrophilic chains. If donor (acceptor) molecules are substituted with alkyl chains and acceptor (donor) molecules with hydrophilic oxyethylene chains, they are not miscible but macroscopically segregated [27]. How do we access the thermodynamic self-sorted nanostructure? The clue is hidden in the amphiphilic molecular design used in previous works, including ours [28–32]. $PDI_{C12/TEG}$ (Figure 2) is a Janus-type amphiphilic compound forming a columnar LC phase at room temperature. $PDI_{C12/TEG}$ molecules pack into the rectangular columnar phase with $p2mg$ symmetry to minimize the unfavorable contact among immiscible hydrophobic and hydrophilic side chains incorporated in a single PDI core. When H_2Pc , a compound carrying hydrophobic chains, is blended with $PDI_{C12/TEG}$, H_2Pc molecules may not intercalate into a column of $PDI_{C12/TEG}$ to avoid the

enthalpic penalty of increasing contacts between hydrophobic and hydrophilic segments. Nevertheless, they are macroscopically miscible with one another due to their hydrophobic chains. We expected that H_2Pc molecules would form a homo-stacked columnar assembly and laterally contact with the hydrophobic chains of $PDI_{C12/TEG}$, resulting in the self-sorted columnar assembly (Figure 1b). The preferential formation of a self-sorted nanostructure will be discussed in detail in the section of Results and Discussion.

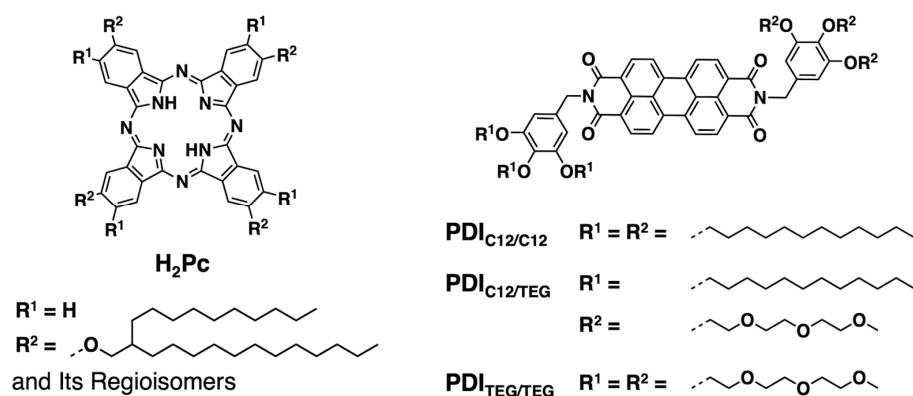


Figure 2. Chemical structures of liquid crystalline phthalocyanine H_2Pc and perylene diimides $PDI_{C12/C12}$, $PDI_{C12/TEG}$, and $PDI_{TEG/TEG}$.

2. Materials and Methods

2.1. Synthesis and Characterization of H_2Pc and PDIs

H_2Pc , $PDI_{C12/C12}$, $PDI_{C12/TEG}$, and $PDI_{TEG/TEG}$ were synthesized according to the previous reports [31,33], and characterized by 1H NMR spectroscopy in $CDCl_3$ on a Varian model Mercury 400 spectrometer, operating at 400 MHz, where chemical shifts were determined with respect to tetramethylsilane as an internal reference. MALDI-TOF mass spectrometry was performed on an Autoflex III spectrometer from Bruker, Japan, using dithranol as a matrix. In addition, 1:1 molar ratio mixtures of H_2Pc and PDI derivatives were prepared from their CH_2Cl_2 solutions in a glass vial. The solvent was evaporated in each solution, allowing for as-prepared waxy LC mixture.

2.2. Characterization of LC Mesophases

The optical textures were recorded by a BX53-P polarizing optical microscope (POM) from Olympus, Japan, equipped with an EOS kiss X7i digital camera from Canon, Japan. The sample was loaded, by use of a capillary action, into an LC cell without any surface treatment. The LC cell was prepared as follows. The glasses with a size of $16 \times 22 \times 0.5$ mm were purchased from Matsunami Glass Ind., Ltd. (Haemacytomer Cover Glasses), Osaka, Japan. Silica beads with 5 μm diameter were dispersed in a drop of fast curing optical adhesive (NOA81) purchased from THORLABS, and the beads-dispersed adhesive was spotted at four places in a rectangle on one glass. Another glass was placed onto the adhesive-spotted glass with a few millimeter offset along with the long axis. The sandwiched glass cell was irradiated with 365 nm light from a SLUV-4 handy UV lamp purchased from AS ONE, Japan, to complete the curing of the adhesive.

The temperature of the sample was controlled by a HS82 hot-stage from Mettler Toledo, Japan. Differential scanning calorimetry (DSC) measurements were performed on a DSC 822e differential scanning calorimeter from Mettler Toledo, Japan. Cooling and heating profiles were recorded and analyzed with the STARe system. Samples were put into an aluminum pan and allowed to be measured under N_2 gas flow.

X-ray diffraction measurements were carried out using a synchrotron radiation X-ray beam with a wavelength of 0.108 nm on BL44B2 at the Super Photon Ring (SPring-8, Hyogo, Japan) [34]. A large Debye–Scherrer camera was used in conjunction with an imaging plate as a detector, and all diffraction patterns were recorded with a 0.01° step in 2θ . The samples were loaded by capillary action at the isotropic liquid melts into a 0.5 mm thick soda glass

capillary purchased from WJM-Glas/Muller GmbH. During the measurements, samples were continuously rotated along the capillary axis to obtain a homogeneous diffraction pattern. The exposure time to the X-ray beam was 1.5 min each.

2.3. Evaluation of Intracolumnar Molecular Order

Electronic absorption spectra were recorded on a V-730 UV/VIS/NIR spectrophotometer from JASCO, Japan, where the scan rate, response, and band width were set at 1000 nm min^{-1} , 0.06 s, and 1.0 nm. The CHCl_3 solution samples were prepared at $2.0 \times 10^{-5} \text{ M}$ and measured in a quartz cell equipped with a screw cap. The optical path length of the cell is 1.0 cm. Spin-coated films were prepared from CHCl_3 solutions of the single compound or 1:1 molar ratio H_2Pc /PDI mixtures onto a quartz substrate with a size of $9 \times 40 \times 1 \text{ mm}$. The spin-coating was performed at 1500 rpm for 30 s using a Mikasa model MS B-100 spin coater.

3. Results and Discussion

3.1. Homeotropic Alignment Capability of H_2Pc and PDIs

The phase transition behaviors of H_2Pc , $\text{PDI}_{\text{C12/C12}}$, $\text{PDI}_{\text{C12/TEG}}$, and $\text{PDI}_{\text{TEG/TEG}}$ were characterized by DSC (Figure S1). They all showed LC mesophases and their clearing points are 180, 223, 189, and $165 \text{ }^\circ\text{C}$ on cooling, respectively, which is almost identical with the previous reports [31,33]. A spontaneous homeotropic alignment of discotic columnar LCs was often reported for hexagonal columnar mesophases [35–38]. The homeotropic alignment capability of H_2Pc discotic columns was already reported in a previous study [39]. The capability of spontaneous homeotropic alignment for the PDI derivatives was monitored by means of POM using samples.

After being loaded into the glass cell with a capillary action at the isotropic liquid phase (Iso), the sample was slowly cooled at 1.0 K/min . Then, the growth of dendritic textures was observed without a polarizer for all the PDI derivatives at around their clearing points (Figure 3a–c). At the same time, no optical texture appeared under crossed polarizers (Figure 3a–c). A similar behavior was seen for H_2Pc with slow cooling at 1.0 K/min (Figure 3d), while defect areas with homogeneous alignment were confirmed upon rapid cooling at 10 K/min (Figure S2). These microscopic observations indicate the strong homeotropic tendency for the hexagonally arranged discotic columns from all four compounds (Figure 3e). Interestingly, after the phase transition from a hexagonal to rectangular columnar mesophase at around $110 \text{ }^\circ\text{C}$ upon cooling, the micrograph of $\text{PDI}_{\text{C12/TEG}}$ was almost unchanged, suggesting that the homeotropic orientation was kept upon the hexagonal–rectangular structural transformation.

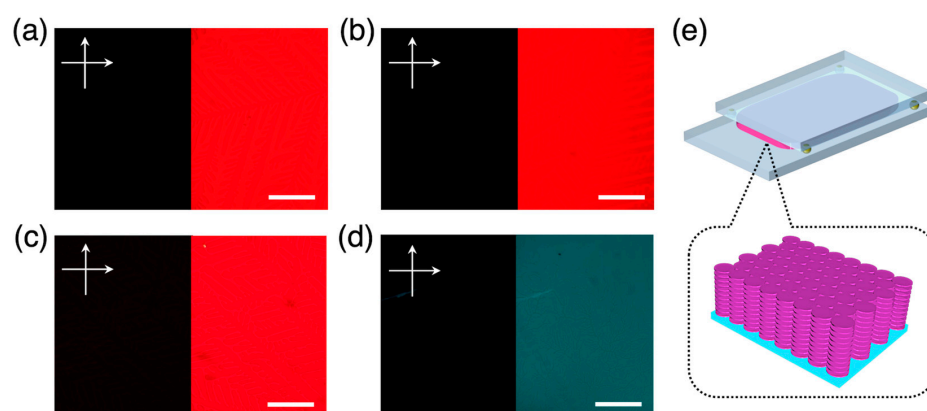


Figure 3. Crossed polarized (left) and optical (right) microscopy images of (a) $\text{PDI}_{\text{C12/C12}}$, (b) $\text{PDI}_{\text{C12/TEG}}$, (c) $\text{PDI}_{\text{TEG/TEG}}$, and (d) H_2Pc in glass sandwich cell without any treatment. (a–d) were taken at 222, 193, 168, and $181 \text{ }^\circ\text{C}$, respectively, after cooling from their isotropic liquid phases at 1.0 K/min . Scale bars represent $200 \text{ } \mu\text{m}$. (e) Schematic illustration of LC samples in $5 \text{ } \mu\text{m}$ thick sandwiched glass cell and homeotropic alignment of discotic columns formed in LC.

3.2. Orientation, Phase Transition Behavior, and Phase Structure of H_2Pc/PDI Mixtures

In order to confirm our hypothesis of the side-chain labeling strategy, 1:1 molar ratio mixtures of $H_2Pc/PDI_{C12/C12}$, $H_2Pc/PDI_{C12/TEG}$, and $H_2Pc/PDI_{TEG/TEG}$ were prepared and their phase behaviors were characterized. The three blend samples were loaded into a sandwich glass cell over $210\text{ }^\circ\text{C}$, and their optical textures were recorded upon cooling. Figure 4 shows optical micrographs with and without crossed polarizers and the dependence of the optical textures on the cooling rate. The mixture of $H_2Pc/PDI_{TEG/TEG}$ gave the most distinctive picture (Figure 4c,f). Independent of the cooling rate, the mixture clearly gave green and red color areas, which most likely correspond to the domains of H_2Pc and $PDI_{TEG/TEG}$, respectively. The hydrophobic H_2Pc and hydrophilic $PDI_{TEG/TEG}$ are immiscible with each other and segregated macroscopically [27]. In contrast, $H_2Pc/PDI_{C12/C12}$ and $H_2Pc/PDI_{C12/TEG}$ appear to have a homogeneous phase in the field of microscope view. Upon rapid cooling from their isotropic phases, fan-shaped textures appeared in POM upon Iso-to-LC phase transitions for both $H_2Pc/PDI_{C12/C12}$ and $H_2Pc/PDI_{C12/TEG}$ (Figure 4a,b). The presence of textures indicates a non-homeotropic alignment of columnar structures. In contrast, the cooling rate was set at 1.0 K/min , and the growth of dendritic textures was seen in optical microscopy without polarizers, but almost dark field images were obtained under crossed polarizers (Figure 4d,e). Although the dark area ratio in these blends was a bit smaller than their constituent compounds, the homeotropic alignment capability was confirmed by POM observations.

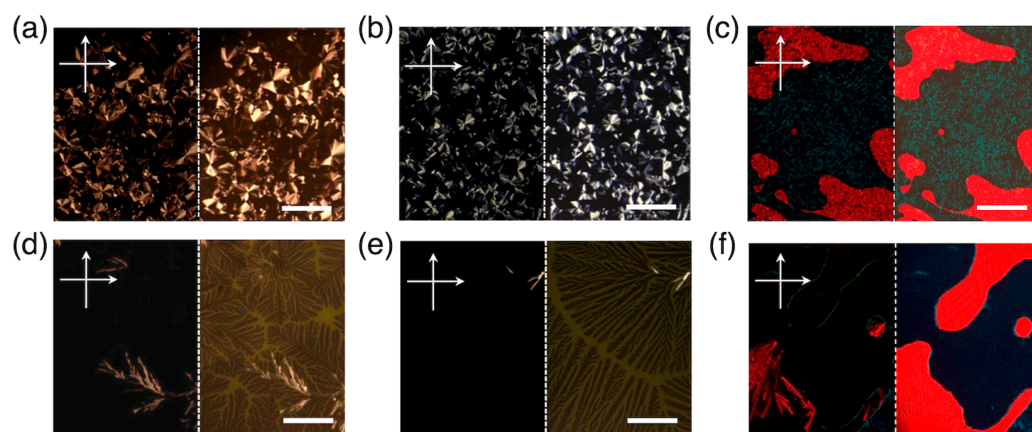


Figure 4. Crossed polarized (left) and optical (right) microscopy images of 1:1 molar ratio mixtures of (a,d) $H_2Pc/PDI_{C12/C12}$, (b,e) $H_2Pc/PDI_{C12/TEG}$, and (c,f) $H_2Pc/PDI_{TEG/TEG}$ in glass sandwich cell without any treatment. Images (a–c) were taken at $25\text{ }^\circ\text{C}$ after rapid cooling from their isotropic melt. (d–f) were taken at 198, 200, and $161\text{ }^\circ\text{C}$, respectively, after cooling from their isotropic liquid phases at 1.0 K/min . Scale bars represent $200\text{ }\mu\text{m}$.

The phase transition behaviors of the 1:1 molar ratio mixture of $H_2Pc/PDI_{C12/C12}$, $H_2Pc/PDI_{C12/TEG}$, and $H_2Pc/PDI_{TEG/TEG}$ were characterized by DSC. The DSC traces of $H_2Pc/PDI_{C12/C12}$ and $H_2Pc/PDI_{C12/TEG}$ implied phase transitions from a mesoscopically uniform material (Figure 5). In the blend of $H_2Pc/PDI_{C12/C12}$, the clearing point ($202\text{ }^\circ\text{C}$ on cooling) is between H_2Pc ($180\text{ }^\circ\text{C}$) and $PDI_{C12/C12}$ ($223\text{ }^\circ\text{C}$) (Figures 5a and S1), which is reasonable for molecularly miscible binary mixtures. In contrast, the clearing point of $H_2Pc/PDI_{C12/TEG}$ ($205\text{ }^\circ\text{C}$ on heating) is higher than those of H_2Pc ($181\text{ }^\circ\text{C}$) and $PDI_{C12/TEG}$ ($191\text{ }^\circ\text{C}$) (Figures 5b and S1). This pattern is quite rare and interesting to note—the LC phase of the blend is thermodynamically more stable than the parent columnar phases. We will discuss this phenomenon in more depth with the powder X-ray diffraction (PXRD) patterns (vide infra). In the blend of $H_2Pc/PDI_{TEG/TEG}$, the melting and clearing points of both the compounds are detected, though the clearing point at $192\text{ }^\circ\text{C}$ is higher than that of H_2Pc ($181\text{ }^\circ\text{C}$) (Figures 5 and S1). In other words, $H_2Pc/PDI_{TEG/TEG}$ affords the superimposed DSC chart of those of the constituent compounds. This is solely a sign of

the macroscopic phase separation of H_2Pc and $\text{PDI}_{\text{TEG}/\text{TEG}}$, which is consistent with the POM images.

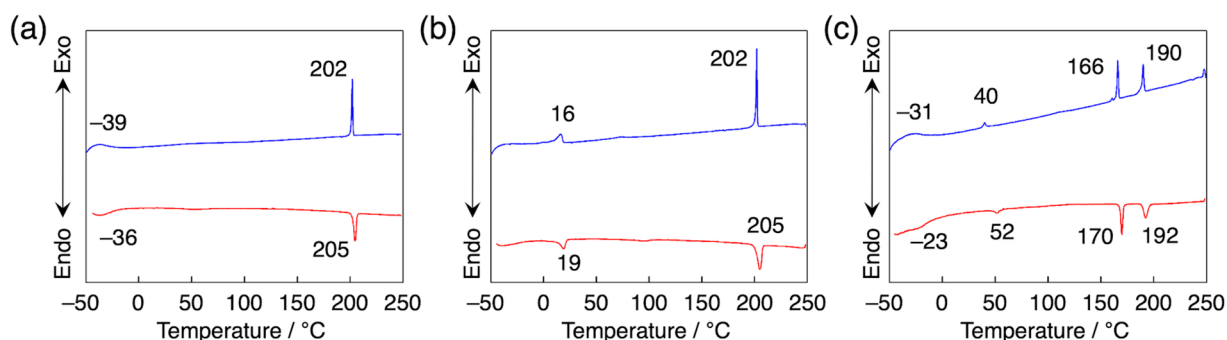


Figure 5. DSC traces of 1:1 molar ratio mixtures of (a) $\text{H}_2\text{Pc}/\text{PDI}_{\text{C12}/\text{C12}}$, (b) $\text{H}_2\text{Pc}/\text{PDI}_{\text{C12}/\text{TEG}}$, and (c) $\text{H}_2\text{Pc}/\text{PDI}_{\text{TEG}/\text{TEG}}$ on 2nd heating/cooling cycle at 10 K/min.

Although the clearing points for $\text{H}_2\text{Pc}/\text{PDI}_{\text{C12}/\text{C12}}$ and $\text{H}_2\text{Pc}/\text{PDI}_{\text{C12}/\text{TEG}}$ are almost identical, the values of phase transition enthalpy inform that the LC phase structure and degree of miscibility are completely different between these mixtures. The LC-to-Iso phase transition enthalpy changes (ΔH) were evaluated from the second heating trace in DSC (Figure S1) and are 4.8, 17.3, and 8.1 kJ mol^{-1} for H_2Pc , $\text{PDI}_{\text{C12}/\text{C12}}$, and $\text{PDI}_{\text{C12}/\text{TEG}}$, respectively. The entropy changes upon these phase transitions (ΔS) can be estimated from the principle that Gibbs free energy is constant upon phase transition, i.e., $\Delta G = \Delta H - T\Delta S = 0$, where ΔG and T are Gibbs free energy change and absolute temperature. By substituting the evaluated ΔH and observed T into the above equation, the values of ΔS were estimated as 10.6, 34.8, and 17.4 $\text{J mol}^{-1} \text{K}^{-1}$ for H_2Pc , $\text{PDI}_{\text{C12}/\text{C12}}$, and $\text{PDI}_{\text{C12}/\text{TEG}}$, respectively. These values well explain the relatively larger entropic gain of linear dodecyloxy chains upon phase transition from columnar mesophase to isotropic liquid. The values of ΔH and ΔS are calculated for the 1:1 molar mixtures of $\text{H}_2\text{Pc}/\text{PDI}_{\text{C12}/\text{C12}}$ and $\text{H}_2\text{Pc}/\text{PDI}_{\text{C12}/\text{TEG}}$ in a similar way, except that the average molecular weight of the two components is used for transforming the observed heat change into enthalpy values. The values of ΔS were estimated as 18.9 and 15.9 $\text{J mol}^{-1} \text{K}^{-1}$ for $\text{H}_2\text{Pc}/\text{PDI}_{\text{C12}/\text{C12}}$ and $\text{H}_2\text{Pc}/\text{PDI}_{\text{C12}/\text{TEG}}$, respectively. The value of 18.9 $\text{J mol}^{-1} \text{K}^{-1}$ for $\text{H}_2\text{Pc}/\text{PDI}_{\text{C12}/\text{C12}}$ is smaller than the averaged ΔS values calculated from those of the parent compound (22.7 $\text{J mol}^{-1} \text{K}^{-1}$), implying that the molecules are disordered in the observed columnar mesophase. For example, one column is composed of H_2Pc and $\text{PDI}_{\text{C12}/\text{C12}}$ molecules. In contrast, the value of 15.9 $\text{J mol}^{-1} \text{K}^{-1}$ for $\text{H}_2\text{Pc}/\text{PDI}_{\text{C12}/\text{TEG}}$ is a bit larger than and even close to the averaged ΔS values of the parent compound (14.0 $\text{J mol}^{-1} \text{K}^{-1}$). This similarity in the entropy values indicates the possibility that H_2Pc and $\text{PDI}_{\text{C12}/\text{TEG}}$ form their respective microdomains. The molecular motion in the microdomains upon the phase transition would be consistent with that in the bulk of the corresponding compounds, while that at the interfaces of the microdomains is relatively limited. In this case, the ΔS value is expected to be smaller than the average values speculated from those for the parent compounds. Considering that the phase transition temperatures for these blends and parent compounds are close and in the range of 181–224 $^{\circ}\text{C}$, the above speculations would have a certain level of significance. As below, we will directly discuss the molecular packing structures in the mesophase for LC blends based on the PXRD measurements.

The molecular packing structures in the mesophases were studied by means of PXRD measurements. In the mesophase at 80 $^{\circ}\text{C}$, the 1:1 molar ratio mixture of $\text{H}_2\text{Pc}/\text{PDI}_{\text{C12}/\text{C12}}$ gave a diffraction pattern that is assignable to a hexagonal columnar phase with the lattice parameter of $a = 32.1 \text{ \AA}$ (Figure 6a). Variable-temperature PXRD measurements elucidated that the hexagonal columnar mesophase was present at 30–200 $^{\circ}\text{C}$ (Figure S4). The parent hexagonal columnar mesophases of H_2Pc and $\text{PDI}_{\text{C12}/\text{C12}}$ have a lattice parameter of $a = \sim 32 \text{ \AA}$ and $\sim 31 \text{ \AA}$, respectively (Figures S3 and S7). The size matching of these two

molecules may be one of the critical reasons for stabilizing a uniform hexagonal packing of mixed-stacked columns. With the clearing temperature information discussed in the DSC section, we conclude that the $\text{H}_2\text{Pc}/\text{PDI}_{\text{C12/C12}}$ self-organized into molecularly miscible, entropically favored columns with hexagonal packing, as illustrated in Figure 7a. Interestingly, the mixture of $\text{H}_2\text{Pc}/\text{PDI}_{\text{C12/TEG}}$ showed different behavior. Over 80°C , the mixture formed a hexagonal columnar phase with $a = \sim 32 \text{ \AA}$ (Figure S5). When being cooled down to 80°C , the mixture changed its PXRD pattern to the superposition of those of H_2Pc and $\text{PDI}_{\text{C12/TEG}}$ (Figure 6b), and similar superimposed patterns were also recorded at 50 and 30°C (Figure S5). Namely, H_2Pc and $\text{PDI}_{\text{C12/TEG}}$ are mesoscopically segregated but macroscopically miscible, as disclosed by PXRD and DSC measurements. The schematic illustration of $\text{H}_2\text{Pc}/\text{PDI}_{\text{C12/TEG}}$ is shown in Figure 7b. Then, we tried to interpret the hexagonal columnar mesophase of $\text{H}_2\text{Pc}/\text{PDI}_{\text{C12/TEG}}$ over 80°C . Although a set of observed diffractions was assigned to a single hexagonal lattice, the (001) peak at $d = \sim 3.4 \text{ \AA}$, corresponding to the π -distance periodicity of $\text{PDI}_{\text{C12/TEG}}$, obviously appeared as similar to those at 30 – 80°C . In addition, as mentioned in the DSC analysis earlier, the clearing temperature of the mixture at 205°C is higher than those of the parent compounds. Having these results in mind, we consider that H_2Pc and $\text{PDI}_{\text{C12/TEG}}$ mainly form self-sorted columns even over 80°C but the average domain size may be decreased. The blend $\text{H}_2\text{Pc}/\text{PDI}_{\text{TEG/TEG}}$ exhibited superimposed patterns of those of H_2Pc and $\text{PDI}_{\text{TEG/TEG}}$ below 240°C (Figures 6 and S6). These results are consistent with the macroscopic phase separation derived from the POM and DSC results. The illustration of macroscopically phase-separated columnar phases is shown in Figure 7c.

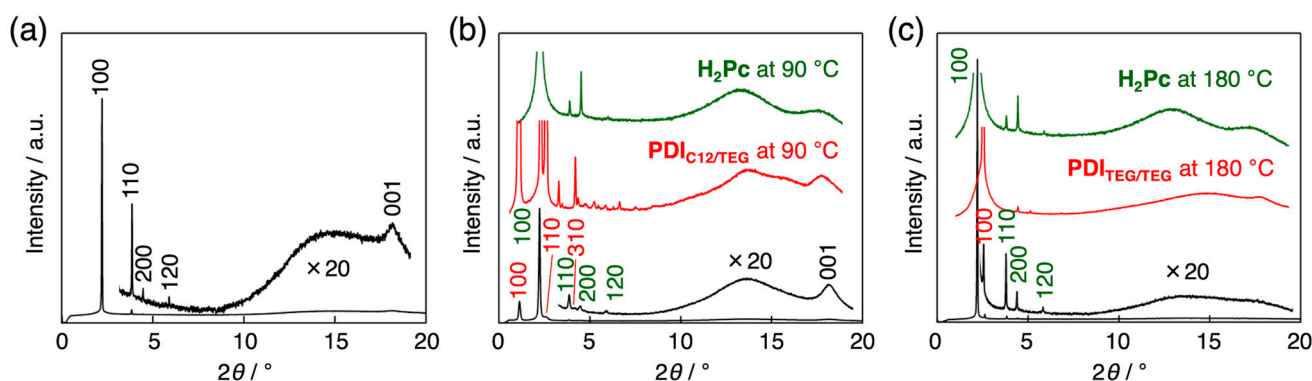


Figure 6. XRD patterns of 1:1 molar ratio mixtures of (a) $\text{H}_2\text{Pc}/\text{PDI}_{\text{C12/C12}}$ at 80°C , (b) $\text{H}_2\text{Pc}/\text{PDI}_{\text{C12/TEG}}$ at 80°C , and (c) $\text{H}_2\text{Pc}/\text{PDI}_{\text{TEG/TEG}}$ at 160°C . For comparison, the XRD patterns of the components for the blends are represented in (b,c).

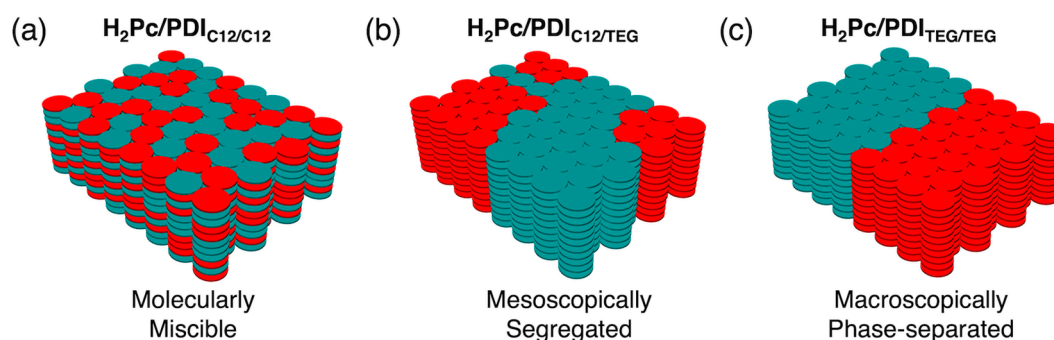


Figure 7. Schematic illustrations of proposed molecular assembly in columnar LC phases for (a) $\text{H}_2\text{Pc}/\text{PDI}_{\text{C12/C12}}$, (b) $\text{H}_2\text{Pc}/\text{PDI}_{\text{C12/TEG}}$, and (c) $\text{H}_2\text{Pc}/\text{PDI}_{\text{TEG/TEG}}$. Red and green disks represent corresponding H_2Pc and PDI molecules.

3.3. Intracolumnar Molecular Order in H_2Pc/PDI Mixtures

The intracolumnar molecular order in the mesophases at room temperature was investigated by absorption spectroscopy of the thin film of the 1:1 molecular blends. In diluted $CHCl_3$ solutions, both H_2Pc and $PDI_{C12/C12}$ are molecularly dispersed and show characteristic absorption at 600–750 nm and 400–550 nm, respectively, with strong vibronic coupling features (Figure 8a). In spin-coated LC films, these absorption bands become broad and blue-shifted due to the columnar assembly of molecules with π - π interactions (H-like aggregation). The spectra of $PDI_{C12/TEG}$ and $PDI_{TEG/TEG}$ in the films are essentially the same as that of $PDI_{C12/C12}$. Then, the spectra of the blend films were analyzed similarly. As expected, in the macroscopically phase-separated $H_2Pc/PDI_{TEG/TEG}$ blend film, the shape of the absorption spectra is almost the superposition of those of the parent LC films (Figures 8b and S8). The heterotropic interactions hardly work due to the limited area of the interfaces between H_2Pc and $PDI_{TEG/TEG}$. In the LC phase of $H_2Pc/PDI_{C12/C12}$, proposed as a molecularly miscible columnar phase, the absorption spectrum of the film is completely different from that of $H_2Pc/PDI_{TEG/TEG}$. The characteristic two intense absorption bands from H_2Pc and $PDI_{C12/C12}$ both show vibronic structures in the blend film, while these bands are broadened compared to their solution states (Figure 8b). This feature strongly indicates that homotropic molecular interactions in their columnar assembly are broken, supporting the proposed molecularly miscible columnar phase (Figure 7a). The film of the $H_2Pc/PDI_{C12/TEG}$ mixture afforded basically the superimposed spectrum of those of H_2Pc and $PDI_{C12/TEG}$. However, shoulder vibronic peaks at around 670–730 nm suggest that a small part of H_2Pc columnar assemblies is dissociated by the intercalation of $PDI_{C12/TEG}$. Thus, the picture of mesoscopically segregated self-sorted assembly as illustrated in Figure 7b may almost be correct, but the structural purity is less than perfect.

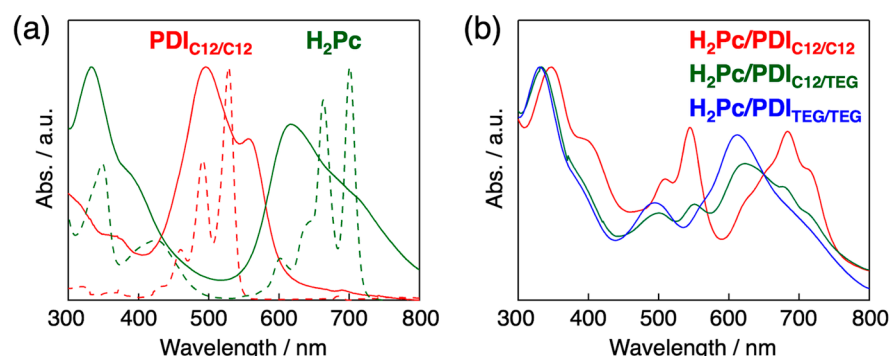


Figure 8. (a) Absorption spectra of H_2Pc (green) and $PDI_{C12/C12}$ (red) in spin-coated film (solid line) and in $CHCl_3$ (dotted line). (b) Absorption spectra of spin-coated film of $H_2Pc/PDI_{C12/C12}$ (red), $H_2Pc/PDI_{C12/TEG}$ (green), and $H_2Pc/PDI_{TEG/TEG}$ (blue).

4. Conclusions

Although nanosegregated, bicontinuous structures of electron-donating and accepting π -conjugated molecules have been recognized as important for photoconducting and photovoltaic properties, only the kinetic control of such nanostructures has been reported so far. We conceived the side-chain labeling strategy using hydrophobic/hydrophilic chains to induce the homotropic self-assembly of donor and acceptor molecules and demonstrated the preferential formation of donor/acceptor self-sorted columnar structures in thermodynamically stable LC binary mixtures. In this LC blend, the columnar mesophases of H_2Pc and PDI molecules are macroscopically miscible and uniform but mesoscopically segregated as evidenced by DSC and PXRD results. In addition, the intercalation of PDI (H_2Pc) to the H_2Pc (PDI) columns is minimally inhibited as supported by absorption spectroscopy. In a more comprehensive view, self-sorted nanostructures of binary mixtures are entropically unfavored in general, but the present work clarified that they can be accessed thermodynamically by self-assembly processes with the help of enthalpic interactions of

immiscible side-chain pairs. Amphiphilic molecules—PDI_{C12}/TEG in this work—induce mesoscopic phase separation and avoid macroscopic phase separation. This role is referred to as a compatibilizer in the research field of macromolecules [40]. While a small molecular compatibilizer has recently been reported [41], our work further extends the concept to the strategy of accessing self-sorted nanostructures. In future, the important subjects include the analysis and control of the size of donor and acceptor nano(micro)-domains, which will lead to the manipulation of photo and electronic functions originating from nanosegregated donor/acceptor blends.

Supplementary Materials: The following supporting information can be downloaded at: <https://www.mdpi.com/article/10.3390/cryst13101473/s1>, Figure S1: DSC traces of H₂Pc, PDI_{C12}/C12, PDI_{C12}/TEG, and PDI_{TEG}/TEG; Figure S2: Crossed polarized microscopy images of H₂Pc in glass sandwich cell; Figure S3: Variable-temperature XRD patterns of H₂Pc; Figure S4: Variable-temperature XRD patterns of 1:1 molar ratio mixture of H₂Pc/PDI_{C12}/C12; Figure S5: Variable-temperature XRD patterns of 1:1 molar ratio mixture of H₂Pc/PDI_{C12}/TEG; Figure S6: Variable-temperature XRD patterns of 1:1 molar ratio mixture of H₂Pc/PDI_{TEG}/TEG; Figure S7: Schematic illustrations of columnar hexagonal and rectangular phases with corresponding lattice parameters and primary diffractions.

Author Contributions: T.S. conceived and designed the experiments; T.S. performed the experiments; T.S. and K.K. analyzed the data; T.S. and M.S. wrote the manuscript draft; K.K. revised the manuscript draft. All authors have read and agreed to the published version of the manuscript.

Funding: This research was funded by JSPS KAKENHI numbers 20H02710 from the Japan Society for the Promotion of Science and a research grant from TEPCO Memorial Foundation.

Data Availability Statement: Not applicable.

Acknowledgments: The synchrotron radiation XRD experiments were performed at BL44B2 in SPring-8 with the approval of RIKEN. T.S. thanks the Leading Initiative for Excellent Young Researchers program by Ministry of Education, Culture, Sports, Science and Technology (MEXT), Japan.

Conflicts of Interest: The authors declare no conflict of interest.

References

1. Robeson, L.M. *Polymer Blends: A Comprehensive Review*; Hanser Publishers: Munich, Germany, 2007.
2. Paul, D.R. *Polymer Blends*; Elsevier: Amsterdam, The Netherlands, 2012; Volume 1.
3. Thomas, S.; Grohens, Y.; Jyotishkumar, P. *Characterization of Polymer Blends: Miscibility, Morphology and Interfaces*; John Wiley & Sons: Hoboken, NJ, USA, 2014.
4. Barlow, J.W.; Paul, D.R. Polymer blends and alloys—A review of selected considerations. *Polym. Sci. Eng.* **1981**, *21*, 985–996. [[CrossRef](#)]
5. Yu, G.; Gao, J.; Hummelen, J.C.; Wudl, F.; Heeger, A.J. Polymer photovoltaic cells: Enhanced efficiencies via a network of internal donor-acceptor heterojunctions. *Science* **1995**, *270*, 1789–1791. [[CrossRef](#)]
6. Dennler, G.; Scharber, M.C.; Brabec, C.J. Polymer-Fullerene Bulk-Heterojunction Solar Cells. *Adv. Mater.* **2009**, *21*, 1323–1338. [[CrossRef](#)]
7. Brabec, C.J.; Gowrisanker, S.; Halls, J.J.M.; Laird, D.; Jia, S.; Williams, S.P. Polymer-Fullerene Bulk-Heterojunction Solar Cells. *Adv. Mater.* **2010**, *22*, 3839–3856. [[CrossRef](#)]
8. Lee, C.; Lee, S.; Kim, G.-U.; Lee, W.; Kim, B.J. Recent Advances, Design Guidelines, and Prospects of All-Polymer Solar Cells. *Chem. Rev.* **2019**, *119*, 8028–8086. [[CrossRef](#)]
9. Xu, C.; Zhao, Z.; Yang, K.; Niu, L.; Ma, X.; Zhou, Z.; Zhang, X.; Zhang, F. Recent progress in all-small-molecule organic photovoltaics. *J. Mater. Chem. A* **2022**, *10*, 6291–6329. [[CrossRef](#)]
10. Gao, H.; Sun, Y.; Meng, L.; Han, C.; Wan, X.; Chen, Y. Recent Progress in All-Small-Molecule Organic Solar Cells. *Small* **2023**, *19*, e2205594. [[CrossRef](#)]
11. Wu, X.; Tam, T.L.D.; Chen, S.; Salim, T.; Zhao, X.; Zhou, Z.; Lin, M.; Xu, J.; Loo, Y.-L.; Leong, W.L. All-Polymer Bulk-Heterojunction Organic Electrochemical Transistors with Balanced Ionic and Electronic Transport. *Adv. Mater.* **2022**, *34*, e2206118. [[CrossRef](#)]
12. Cheng, S.-S.; Huang, P.-Y.; Ramesh, M.; Chang, H.-C.; Chen, L.-M.; Yeh, C.-M.; Fung, C.-L.; Wu, M.-C.; Liu, C.-C.; Kim, C.; et al. Solution-Processed Small-Molecule Bulk Heterojunction Ambipolar Transistors. *Adv. Funct. Mater.* **2014**, *24*, 2057–2063. [[CrossRef](#)]
13. Sugiyasu, K.; Kawano, S.; Fujita, N.; Shinkai, S. Self-Sorting Organogels with p-n Heterojunction Points. *Chem. Mater.* **2008**, *20*, 2863–2865. [[CrossRef](#)]

14. Molla, M.R.; Das, A.; Ghosh, S. Chiral induction by helical neighbour: Spectroscopic visualization of macroscopic-interaction among self-sorted donor and acceptor π -stacks. *Chem. Commun.* **2011**, *47*, 8934–8936. [[CrossRef](#)] [[PubMed](#)]
15. Prasanthkumar, S.; Ghosh, S.; Nair, V.C.; Saeki, A.; Seki, S.; Ajayaghosh, A. Organic Donor–Acceptor Assemblies form Coaxial p–n Heterojunctions with High Photoconductivity. *Angew. Chem. Int. Ed.* **2015**, *54*, 946–950. [[CrossRef](#)] [[PubMed](#)]
16. Draper, E.R.; Lee, J.R.; Wallace, M.; Jäckel, F.; Cowan, A.J.; Adams, D.J. Self-sorted photoconductive xerogels. *Chem. Sci.* **2016**, *7*, 6499–6505. [[CrossRef](#)] [[PubMed](#)]
17. Seki, A.; Yoshio, M.; Mori, Y.; Funahashi, M. Ferroelectric Liquid-Crystalline Binary Mixtures Based on Achiral and Chiral Trifluoromethylphenylterthiophenes. *ACS Appl. Mater. Interfaces* **2020**, *12*, 53029–53038. [[CrossRef](#)] [[PubMed](#)]
18. Zhang, C.; Nakano, K.; Nakamura, M.; Araoka, F.; Tajima, K.; Miyajima, D. Noncentrosymmetric Columnar Liquid Crystals with the Bulk Photovoltaic Effect for Organic Photodetectors. *J. Am. Chem. Soc.* **2020**, *142*, 3326–3330. [[CrossRef](#)] [[PubMed](#)]
19. Franca, L.G.; Dos Santos, P.L.; Pander, P.; Cabral, M.G.B.; Cristiano, R.; Cazati, T.; Monkman, A.P.; Bock, H.; Eccher, J. Delayed Fluorescence by Triplet-Triplet Annihilation from Columnar Liquid Crystal Films. *ACS Appl. Electron. Mater.* **2022**, *4*, 3486–3494. [[CrossRef](#)]
20. Yang, Z.; Li, J.; Chen, X.; Fan, Y.; Huang, J.; Yu, H.; Yang, S.; Chen, E.-Q. Precisely Controllable Artificial Muscle with Continuous Morphing based on “Breathing” of Supramolecular Columns. *Adv. Mater.* **2023**, *35*, e2211648. [[CrossRef](#)]
21. Nunes da Silva, F.; Marchi Luciano, H.; Stadlober, C.H.; Farias, G.; Durola, F.; Eccher, J.; Bechtold, I.H.; Bock, H.; Gallardo, H.; Vieira, A.A. Columnar Liquid Crystalline Glasses by Combining Configurational Flexibility with Moderate Deviation from Planarity: Extended Triaryltriazines. *Chem. Eur. J.* **2023**, *29*, e202203604. [[CrossRef](#)]
22. Takahashi, H.; Kohri, M.; Kishikawa, K. Axially Polar-Ferroelectric Columnar Liquid Crystalline System That Maintains Polarization upon Switching to the Crystalline Phase: Implications for Maintaining Long-Term Polarization Information. *ACS Appl. Nano Mater.* **2023**, *6*, 10531–10538. [[CrossRef](#)]
23. Delage-Laurin, L.; Swager, T.M. Liquid Crystalline Magneto-Optically Active Peralkylated Azacoronene. *JACS Au* **2023**, *3*, 1965–1974. [[CrossRef](#)]
24. Zucchi, G.; Donnio, B.; Geerts, Y.H. Remarkable miscibility between disk- and lathlike mesogens. *Chem. Mater.* **2005**, *17*, 4273–4277. [[CrossRef](#)]
25. Zucchi, G.; Viville, P.; Donnio, B.; Vlad, A.; Melinte, S.; Mondeshki, M.; Graf, R.; Spiess, H.W.; Geerts, Y.H.; Lazzaroni, R. Miscibility between Differently Shaped Mesogens: Structural and Morphological Study of a Phthalocyanine-Perylene Binary System. *J. Phys. Chem. B* **2009**, *113*, 5448–5457. [[CrossRef](#)]
26. Sakurai, T.; Yoneda, S.; Sakaguchi, S.; Kato, K.; Takata, M.; Seki, S. Donor/Acceptor Segregated π -Stacking Arrays by Use of Shish-Kebab-Type Polymeric Backbones: Highly Conductive Discotic Blends of Phthalocyaninatopolysiloxanes and Perylenediimides. *Macromolecules* **2017**, *50*, 9265–9275. [[CrossRef](#)]
27. Thiebaut, O.; Bock, H.; Grelet, E. Face-on Oriented Bilayer of Two Discotic Columnar Liquid Crystals for Organic Donor-Acceptor Heterojunction. *J. Am. Chem. Soc.* **2010**, *132*, 6886–6887. [[CrossRef](#)] [[PubMed](#)]
28. Sakurai, T.; Shi, K.; Sato, H.; Tashiro, K.; Osuka, A.; Saeki, A.; Seki, S.; Tagawa, S.; Sasaki, S.; Masunaga, H.; et al. Prominent Electron Transport Property Observed for Triply Fused Metalloporphyrin Dimer: Directed Columnar Liquid Crystalline Assembly by Amphiphilic Molecular Design. *J. Am. Chem. Soc.* **2008**, *130*, 13812–13813. [[CrossRef](#)] [[PubMed](#)]
29. Lehmann, M.; Jahr, M.; Gutmann, J. Star-shaped oligobenzoates with a naphthalenechromophore as potential semiconducting liquid crystal materials? *J. Mater. Chem.* **2008**, *14*, 2995–3003. [[CrossRef](#)]
30. Sakurai, T.; Tsutsui, Y.; Choi, W.; Seki, S. Intrinsic Charge Carrier Mobilities at Insulator–Semiconductor Interfaces Probed by Microwave-based Techniques: Studies with Liquid Crystalline Organic Semiconductors. *Chem. Lett.* **2015**, *44*, 1401–1403. [[CrossRef](#)]
31. Sakurai, T.; Tsutsui, Y.; Kato, K.; Takata, M.; Seki, S. Preferential formation of columnar mesophases via peripheral modification of discotic π -systems with immiscible side chain pairs. *J. Mater. Chem. C* **2016**, *4*, 1490–1496. [[CrossRef](#)]
32. Funahashi, M. Anisotropic electrical conductivity of n-doped thin films of polymerizable liquid-crystalline perylene bisimide bearing a triethylene oxide chain and cyclotetrasiloxane rings. *Mater. Chem. Front.* **2017**, *1*, 1137–1146. [[CrossRef](#)]
33. Tant, J.; Geerts, Y.H.; Lehmann, M.; De Cupere, V.; Zucchi, G.; Laursen, B.W.; Bjornholm, T.; Lemaur, V.; Marcq, V.; Burquel, A.; et al. Liquid Crystalline Metal-Free Phthalocyanines Designed for Charge and Exciton Transport. *J. Phys. Chem. B* **2005**, *109*, 20315–20323. [[CrossRef](#)]
34. Kato, K.; Tanaka, Y.; Yamauchi, M.; Ohara, K.; Hatsui, T. A Statistical approach to correct X-ray response non-uniformity in microstrip detectors for high-accuracy and high-resolution total-scattering measurements. *J. Synchrotron Radiat.* **2019**, *26*, 762–773. [[CrossRef](#)]
35. Hatsusaka, K.; Ohta, K.; Yamamoto, I.; Shirai, H. Discotic liquid crystals of transition metal complexes, Part 30: Spontaneous uniform homeotropic alignment of octakis(dialkoxyphenoxy)phthalocyaninatocopper(II) complexes. *J. Mater. Chem.* **2001**, *11*, 423–433. [[CrossRef](#)]
36. Wang, J.; He, Z.; Zhang, Y.; Zhao, H.; Zhang, C.; Kong, X.; Mu, L.; Liang, C. The driving force for homeotropic alignment of a triphenylene derivative in a hexagonal columnar mesophase on single substrates. *Thin Solid Films* **2010**, *518*, 1973–1979. [[CrossRef](#)]
37. Osawa, T.; Kajitani, T.; Hashizume, D.; Ohsumi, H.; Sasaki, S.; Takata, M.; Koizumi, Y.; Saeki, A.; Seki, S.; Fukushima, T.; et al. Wide-Range 2D Lattice Correlation Unveiled for Columnarly Assembled Triphenylene Hexacarboxylic Esters. *Angew. Chem. Int. Ed.* **2012**, *51*, 7990–7993. [[CrossRef](#)] [[PubMed](#)]

38. Kobayashi, Y.; Muranaka, A.; Kato, K.; Saeki, A.; Tanaka, T.; Uchiyama, M.; Osuka, A.; Aida, T.; Sakurai, T. A structural parameter to link molecular geometry to macroscopic orientation in discotic liquid crystals: Study of metalloporphyrin tapes. *Chem. Commun.* **2021**, *57*, 1206–1209. [[CrossRef](#)] [[PubMed](#)]
39. Schweicher, G.; Gbabode, G.; Quist, F.; Debever, O.; Dumont, N.; Sergeev, S.; Geerts, Y.H. Homeotropic and Planar Alignment of Discotic Liquid Crystals: The Role of the Columnar Mesophase. *Chem. Mater.* **2009**, *21*, 5867–5874. [[CrossRef](#)]
40. Self, J.L.; Zervoudakis, A.J.; Peng, X.; Lenart, W.R.; Macosko, C.W.; Ellison, C.J. Linear, Graft, and Beyond: Multiblock Copolymers as Next-Generation Compatibilizers. *JACS Au* **2022**, *2*, 310–321. [[CrossRef](#)]
41. Grimann, M.; Ueberschaer, R.; Tatarov, E.; Fuhrmann-Lieker, T. Phase Separation and Nanostructure Formation in Binary and Ternary Blends of Spiro-Linked Molecular Glasses. *J. Phys. Chem. B* **2020**, *124*, 5507–5516. [[CrossRef](#)]

Disclaimer/Publisher's Note: The statements, opinions and data contained in all publications are solely those of the individual author(s) and contributor(s) and not of MDPI and/or the editor(s). MDPI and/or the editor(s) disclaim responsibility for any injury to people or property resulting from any ideas, methods, instructions or products referred to in the content.